remote sensing

MDPI

Article

Estimates of Power Shortages and Affected Populations during the Initial Period of the Ukrainian-Russian Conflict

Zihao Zheng [1,2], Zhifeng Wu [1,3], Zheng Cao [1,*], Qifei Zhang [1], Yingbiao Chen [1], Guanhua Guo [1], Zhiwei Yang [1], Cheng Guo [1], Xin Wang [4] and Francesco Marinello [2]

1 School of Geography and Remote Sensing, Guangzhou University, Guangzhou 510006, China
2 Department of Land, Environment, Agriculture and Forestry, University of Padova, 35020 Legnaro, Italy
3 MNR Key Laboratory for Geo-Environmental Monitoring of Great Bay Area, Shenzhen 518000, China
4 South China Institute of Environmental Science, Ministry of Ecology and Environment, Guangzhou 510535, China
* Correspondence: jnczdl@gzhu.edu.cn

Abstract: Since the outbreak of the Ukrainian-Russian conflict on 24 February 2022, Ukraine's economy, society, and cities have been devastated and struck on multiple fronts, with large numbers of refugees fleeing to neighboring countries. The lighting systems in Ukrainian cities have been severely restricted due to Russian missile bombing and curfew policies. The power shortages adversely affected the livelihoods of the Ukrainian residents dramatically. For a timely assessment of the power shortages' extent and the affected population in Ukraine, this study tracked the dynamics of nighttime light emissions in Ukraine based on the newly developed daily Black Marble product (VNP46A2) from NASA. The results show that the average light radiance in Ukrainian urban areas has decreased by about 37% since the eruption of the war, with Kiev city being the most dramatic region, having a post-conflict decrease of about 51%. In addition, by introducing near-real-time population data, we have implemented a survey of the affected population in Ukraine suffering from war-induced power shortages. Estimates show that about 17.3 million Ukrainian residents were affected by power shortages. In more detail, the number of children under 10 years old was about 2.35 million (about 5.24% of the total population), while the number of elderly people over 60 years old was about 3.53 million (about 7.86% of the total population). Generally, the results of this study could contribute positively to the timely assessment of the impact of the conflict and the implementation of humanitarian relief.

Keywords: Ukrainian-Russian conflict; VNP46A2; Black Marble; power shortages; population estimation

Citation: Zheng, Z.; Wu, Z.; Cao, Z.; Zhang, Q.; Chen, Y.; Guo, G.; Yang, Z.; Guo, C.; Wang, X.; Marinello, F. Estimates of Power Shortages and Affected Populations during the Initial Period of the Ukrainian-Russian Conflict. *Remote Sens.* **2022**, *14*, 4793. https://doi.org/10.3390/rs14194793

Academic Editor: Bailang Yu

Received: 10 August 2022
Accepted: 22 September 2022
Published: 26 September 2022

1. Introduction

On 24 February 2022, with Russian President Vladimir Putin's military action in Ukraine, the Ukrainian-Russian conflict officially kicked off and the situation changed rapidly [1]. Since the beginning of the conflict, Russia has carried out multi-point military strikes against Ukraine, and armed forces have been deployed in Lugansk and Donetsk oblasts, which are controlled by independent forces, and the border area between Belarus and Ukraine [2]. As the conflict continues, several cities or bases have been seized and controlled by Russia. The Russian-Ukrainian conflict has become another hot topic of global attention after COVID-19 [3]. As the largest military conflict in Europe since the beginning of the 21st century, the Russia-Ukraine conflict has continued to worsen the global and regional security situation.

The conflict has triggered a high number of casualties in Ukraine, with the Office of the UN High Commissioner for Human Rights (OHCHR) recording more than 10,000 civilian casualties as of 3 July 2022, with 335 of the 4889 children involved being killed [4]. In addition, as a concomitant effect, inter-regional sanctions and countersanctions have had a huge impact on international financial markets, energy markets, food markets, etc., making

the global supply chain blockage increasingly serious and casting a shadow on the global economy's sluggish recovery. Compared to the impact on international markets, armed conflict has caused more serious disruptions to the lives and work of local populations and resulted in large numbers of refugees fleeing the fighting. The United Nations High Commissioner for Refugees (UNHCR) has stated that 4.3 million refugees left Ukraine within six weeks of the start of the conflict, and another 7.1 million people were displaced within Ukraine [5].

Since the conflict is still in an ongoing phase, it is difficult to obtain information through traditional ground-based surveys. Non-contact remote sensing techniques have proven to be an effective and low-cost means of investigating armed conflicts. Typically, warfare destroys urban public infrastructure, such as airports, roads, and houses, and leads to dramatic changes in human activities (Figure 1). Nighttime remote light sensing can provide unique spatial observations related to human activities; it has been proven as an effective tool for detecting global armed conflicts [6]. By comparing the variations of artificial light radiation on the ground before and after the war, the dynamics of human activities, power supply, and other elements in conflict areas can be measured in a timely manner. For example, recent studies have investigated the Syrian crisis [7], the Iraqi civil war [8], and the Yemen crisis [9] by using time-series nighttime light remote sensing imagery. These surveys and applications have effectively assessed the adverse effects of war on the livelihoods of regional residents from a new perspective and have positively contributed to the development of humanitarian organizations' relief efforts.

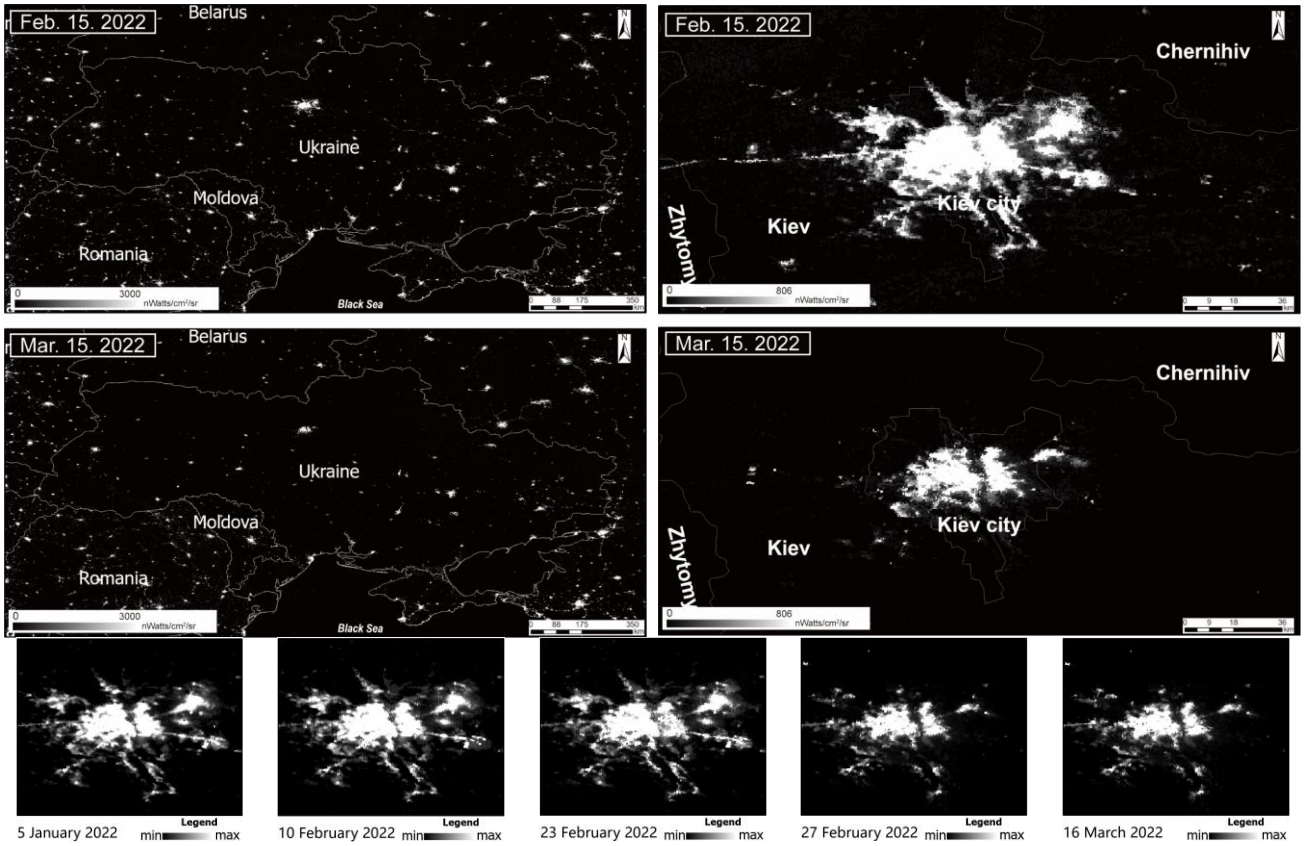

Figure 1. (**a**) A snapshot comparison of regional night lights before and after the Ukrainian-Russian conflict; (**b**) Time-series of light images in Kiev city.

After decades of exploration, nighttime remote light sensing has made great progress, and many achievements have been made regarding data sources, sensor calibration, and applications [7,10–19]. Although the number of sensors in orbit for nighttime observation missions is increasing, the most widely used nighttime remote sensing data today, given

data availability, still comes from the Defense Meteorological Satellite Program Operational Line Scan System (DMSP-OLS) and the Suomi National Polar-Orbiting Partner Visible Infrared Imaging Radiometer Suite (NPP-VIIRS) [20–22]. DMSP-OLS is the longest-operating nighttime light satellite, with products available every year from 1992 to 2013 [23]. However, DMSP-OLS data suffers from coarse spatial resolution (30 arc seconds, about 1000 m at the equator), low radiometric resolution, and lack of on-board radiometric calibration. Later, the National Oceanic and Atmospheric Administration (NOAA) released the next-generation NPP-VIIRS nighttime light product, and the first images were recorded by VIIRS in November 2011, with data available since 2012. Improved performance, including higher spatial resolution (15 arc seconds, about 500 m at the equator), shorter revisit cycles, radiation detection capability, and no saturation in urban areas [24] suggest its greater potential for short-period event applications [25–27].

Due to the excellent performance of the VIIRS sensor, its acquired data was introduced into multiple processing chains to create several ready-to-use products, including monthly composites, annual composites, etc., which provide data support to scientists around the world [21]. One of the most notable is the new Black Marble product, developed by NASA in recent years based on VIIRS data [28]. Black Marble is a suite of products that are calibrated and validated on a daily basis, thus providing new and powerful data support for emergency event monitoring (e.g., disasters, accidents, conflicts, etc.). Recently, applications based on the daily product VNP46A2 from the Black Marble suite are also being initiated, such as the evaluation of power outages caused by hurricanes [29,30] and the analysis of human lifestyle changes during COVID-19 [31,32].

Therefore, in this paper we have taken the current high-profile Ukrainian-Russian conflict as a case to explore the potential of the Black Marble daily product and to expand its application in evaluating war events. Specifically, the daily VNP46A2 light images from the early period of the Ukrainian-Russian conflict (spanning about 88 days) were selected for trend assessment and quantitative analysis to reveal the dynamic characteristics of light radiance. In addition, based on the results of the light dynamics trend, we identified areas where power shortages occurred in the pre-conflict period and combined them with demographic data to predict the population suffering from power shortages. Our study provides a new perspective for understanding the current Ukrainian-Russian conflict and assessing the damage the conflict causes to human activities.

2. Materials and Methods

2.1. Study Area

Ukraine is located in the eastern part of Europe, on the northern coast of the Black Sea and the Sea of Azov. It is bordered by Belarus in the north, Russia in the northeast, Poland, Slovakia and Hungary in the west, and Romania and Moldova in the south. Ukraine is the second-largest country in Europe in terms of territorial area, after Russia, with a population of 44.9 million [33]. Ukraine is divided into 24 oblasts, 1 autonomous republic (the Republic of Crimea), and 2 municipalities (Kiev city and Sevastopol), making a total of 27 first-level administrative regions. Considering that the Crimean Peninsula is disputed and has been under Russian control for a long time, we did not include it as a study area for this case (Figure 2).

Figure 2. Location map of the study area (red highlighted spot in the upper right corner is the location of the Earth view).

2.2. Data Sources

2.2.1. Daily Nighttime Light Data

The analysis of the light radiance is based on the daily moonlight adjusted NTL of NASA's VIIRS Black Marble product (VNP46A2, collection V001). Based on VNP46A1, VNP46A2 enhances its quality with a series of corrections, including lunar BRDF, clouds, topography, atmosphere, airglow, stray light, and significantly enhanced sensitivity to low illumination variations [34]. The product contains seven science data sets (SDSs), of which "Gap-Filled DNB BRDF-Corrected NTL" stores the intensity of the fixed-light radiation. Like the other VIIRS-derived products, VNP46A2 has a spatial resolution of 15 arc seconds (~500 m). More details about VNP46A2 can be found on the official website of Black Marble (https://blackmarble.gsfc.nasa.gov/#home, accessed on 3 August 2022).

Considering that this study is more concerned with power shortages due to military operations in the earlier period of the conflict, eight tiles covering the whole of Ukraine between 20 December 2021 and 17 March 2022, totaling 88 × 8 scenes of VNP46A2 images, were used to track the dynamics of light radiation before and after the conflict.

2.2.2. Spatialized Population Data

In addition, to estimate the population affected by the sharp decrease in illumination, the LandScan HD for Ukraine [35], which was completed and released by the Oak Ridge National Laboratory (ORNL) in January 2022, and the Global Project Population Data (GPPD) [36], which was released by WorldPop, were used in this paper.

Specifically: (1) LandScan HD provides gridded population estimates at a resolution of 3 arc seconds (~100 m). It integrates high-resolution building features, land use, infrastructure, and POI data from various sources, applies occupancy estimates from the ORNL Population Density Table (PDT) project, and uses a novel image-processing algorithm developed by ORNL to rapidly map building structures and neighborhood environments [37,38]. Then, the population spatialized raster was exported by adjusting it to the reference data provided by the National Statistical Service of Ukraine and the CIA World Factbook. More details about LandScan HD for Ukraine can be found via https://landscan.ornl.gov/metadata (accessed on 3 August 2022).

(2) GPPD data from the WorldPop project were derived from detailed mapping of settlements, associating these settlement boundaries with gazetteer population numbers, and employing a random forest regression tree mapping method to accurately map the resident population within the settlements [39]. Compared to the timely and fine-grained population mapping data published by ORNL for Ukraine, the GPPD developed by WorldPop provides the population of Ukraine by age and sex groups in 2020. Although this dataset was not as up to date as LandScan HD for Ukraine, it was also introduced in this paper as it provides population structure details that can be used for subsequent analysis (more details on the population structure profiles can be found at: https://developers.google.com/earth-engine/datasets/catalog/WorldPop_GP_100m_pop_age_sex?authuser=1#bands, accessed on 3 August 2022).

2.2.3. Auxiliary Data

In this paper, some additional vector boundary data derived from Natural Earth were used, including the national boundaries and Ukrainian oblast boundaries. It can be directly downloaded and distributed via https://www.naturalearthdata.com/features/ (accessed on 3 August 2022). In addition, this article collects statistical population reports from the official publications, which are available at the Statistical Service of Ukraine (http://db.ukrcensus.gov.ua/PXWEB2007/popul_eng.htm, accessed on 3 August 2022).

2.3. Methods

2.3.1. Identifying Power Shortage Areas

Previous studies have adequately validated the feasibility of assessing power shortages around emergency events based on NTL satellite products, especially NPP-VIIRS products, which have high temporal and spatial resolution [25,26,30]. Similarly, in this paper, the dramatic decay of nighttime light radiation at the surface was considered an indication that power shortages were occurring.

Since sharp reductions in power lighting can be visually observed in the time-series daily VNP46A2 images (Figure 1b), a straightforward method of identifying power shortages in the early stages of the conflict was to detect dynamic trends in the light pixels. First, to avoid possible abnormal fluctuations and to improve the stability of the conclusions, a 3-day median-filtered sliding window was used to smooth the time series of light images. Then, a simple and efficient trend detection method for time-series data, using Theil–Sen median trend analysis and Mann–Kendall testing, was deployed to obtain the change trends at the pixel level [40,41]. Both methods are highly tolerant of outliers and have been widely deployed for the trend analysis of vegetation, precipitation, air temperature, and other factors [42,43]. The Theil–Sen median trend is calculated as

$$Slope_{NTL} = median\left(\frac{NTL_i - NTL_j}{j - i}\right) \quad (1)$$

where NTL_i and NTL_j are the pixel values of the light images of day i and day j, respectively. The $Slope_{NTL}$ indicates the dynamic trend of the light; if it is greater than 0 it means an increase, while less than 0 means a decrease.

The Mann–Kendall test is calculated as

$$Z = \begin{cases} (S-1)/\sqrt{Var(S)} & \text{if } S > 0 \\ 0 & \text{if } S = 0 \\ (S+1)/\sqrt{Var(S)} & \text{if } S < 0 \end{cases} \quad (2)$$

$$S = \sum_{i=1}^{n-1} \sum_{j=i+1}^{n} sgn\left(NTL_j - NTL_i\right) \quad (3)$$

$$sgn\left(NTL_j - NTL_i\right) = \begin{cases} +1 & \text{if } NTL_j - NTL_i > 0 \\ 0 & \text{if } NTL_j - NTL_i = 0 \\ -1 & \text{if } NTL_j - NTL_i < 0 \end{cases} \quad (4)$$

$$Var(S) = n(n-1)(2n+5)/18 \tag{5}$$

where $sgn(NTL_j - NTL_i)$ is the sign function, n is the days of observation, and Z is the standard normal test statistic. Testing trends is done at the specific α significance level. In this paper, at a confidence level of $\alpha = 0.05$, the null hypothesis of no trend is rejected as $|Z| \geq 1.96$. In addition, to further delineate the magnitude of the trend, $\left|Slope_{\overline{NTL}_{median}}\right|$, which was the median of the significantly declining pixels in the study area, was used as a threshold to group slightly changed and drastically changed pixels. Since the magnitude and volume of the significantly decreased light pixels in Ukraine far exceeded the increased ones, defining the threshold this way could avoid an overestimation of the increased pixels. Equation (6) shows their specific classification, and here we defined "*Dramatically decreased*" as a pixel experiencing a power shortage.

$$Dynamic\ Types = \begin{cases} Dramatically\ increased\ \left(Slope_{NTL} \geq \left|Slope_{\overline{NTL}_{median}}\right|\right) \\ Slightly\ increased\ \left(0 < Slope_{NTL} < \left|Slope_{\overline{NTL}_{median}}\right|\right) \\ Slightly\ decreased\ \left(0 > Slope_{NTL} > \left|Slope_{\overline{NTL}_{median}}\right|\right) \\ Dramatically\ decreased\ \left(Slope_{NTL} \leq \left|Slope_{\overline{NTL}_{median}}\right|\right) \end{cases} \tag{6}$$

2.3.2. Estimation of the Population Exposed to Power Shortages

The impact of the power shortages that accompanied the conflict on the lives and production of the population also cannot be ignored. Timely assessment of populations suffering from light fading or even power shortages is essential to better assessing the adverse effects of war and post-war recovery and humanitarian relief.

- Estimation of total population exposed

As mentioned earlier, LandScan HD for Ukraine provides the most timely high-resolution spatialized population data in Ukraine. Thus, it is used to estimate the total population in areas with power shortages. Specifically, (1) pixels marked as power shortages in the trend analysis results were aggregated and extracted; (2) Based on the spatial statistics tools provided by the ArcGIS Pro platform, the population pixels from the LandScan HD layer corresponding to the locations of the above extracted pixels were zoned and aggregated; (3) Finally, the affected population of each region and the nation was exported.

- Estimation of vulnerable populations

Considering the possible age differences in stress response and adaptive capacity in the face of disasters and war, children younger than 10 years and adults older than 60 years were considered vulnerable populations in this paper [44,45]. Hence, age-stratified profiles provided by the WorldPop GPPD dataset were introduced to estimate the conflict-affected vulnerable population in Ukraine.

First, we evaluated the feasibility of migrating WorldPop GPPD population structure profiles into LandScan HD for Ukraine, due to their inconsistent data acquisition times. Therefore, multiple sample areas of the population clusters were selected, and a linear regression analysis was deployed to assess the correlation between the two datasets based on the correlation coefficients. Next, based on the WorldPop GPPD, the coefficients for the ratio of the population below 10 years and above 60 years were exported according to Equation (7). Finally, these coefficient layers were correlated with LandScan HD for Ukraine population layers to calculate the distribution of vulnerable populations (Equation (8)).

$$\begin{aligned} Ratio_{Pop<10} &= \frac{Pop_{<10}}{Pop_{total}} \\ Ratio_{Pop\geq 60} &= \frac{Pop_{\geq 60}}{Pop_{total}} \end{aligned} \tag{7}$$

$$\begin{aligned} Pop_{<10} &= Ratio_{Pop<10} \times Pop_{LandScan\ HD} \\ Pop_{\geq 60} &= Ratio_{Pop\geq 60} \times Pop_{LandScan\ HD} \end{aligned} \tag{8}$$

where $Pop_{<10}$, $Pop_{\geq 60}$, and Pop_{total} represent the population of children younger than 10 years old, the population aged over 60 years, and the total population, respectively; $Ratio_{Pop<10}$ and $Ratio_{Pop\geq 60}$ are the coefficients corresponding to the vulnerable population.

3. Results

3.1. Dynamics of Light Radiance and Identified Areas

3.1.1. Regional-Scale Dynamics of Light Radiation

Figure 3a shows the nighttime light radiation dynamics at national scale, before and after smoothing, during the observation period. After window smoothing, several transient anomalous fluctuations were filtered, and the NTL dynamic curve was more stabilized. Moreover, it can be observed that the suppression of the mean light radiation on a national scale by the conflict was also very pronounced. For instance, after the outbreak of the conflict (24 February), the average radiance in Ukraine experienced a continuous decrease. According to statistics, the mean observed radiance in Ukraine before the conflict was about 4.64 nWatts/cm^2/sr, while after the conflict the recorded mean radiance decreased to 3.56 nWatts/cm^2/sr, with a drop of about 23%.

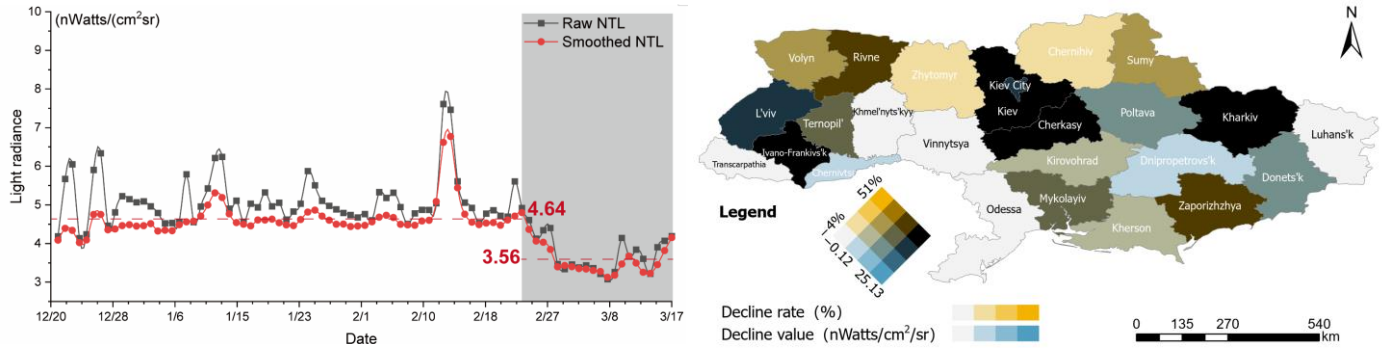

Figure 3. (**a**) Daily mean light radiation curve of Ukraine on the national scale (gray background represents the period of conflict); (**b**) The rate and magnitude of light decay at the oblast scale.

At the oblast scale, we further calculated the rates and magnitudes of light radiance change before (20 December 2021–23 February 2022) and after (1 March 2022–7 March 2022, which was the first plateau phase after the decline in light radiance according to Figure 3a) the conflict. It can be found that Kiev, Kharkiv, Cherkasy, and Ivano-Frankivs'k were the oblasts with the most dramatic and significant reduction of light emissions. Specifically, Kiev's light radiation dropped by about 51% after the conflict, which was the most dramatic area, Kharkiv had the second-largest drop, reaching about 39%, and Cherkasy and Ivano-Frankivs'k were closer at about 35% (Figure 3b). Conversely, Khmel'nyts'ky, Vinnytsya, and Odessa experienced the least decline in light radiation, with all declines of less than 10%.

Considering that the conflict was more intense in urban areas and the resulting power shortages were more severe, the daily mean light radiation dynamics in urban areas of Ukraine before and after the conflict were also calculated based on the urban boundary layers provided by Natural Earth. The results in Figure 4a show that the baseline of light radiation in urban areas has decreased more dramatically compared to the national scale. Before the outbreak of the conflict, the average daily light radiation was about 64.18 nWatts/cm^2/sr, while after the outbreak of the conflict light radiation decreased sharply to 40.30 nWatts/cm^2/sr, a decrease of about 37%. It is worth noting that compared to the national scale, which includes both urban and rural areas, the light curve in urban areas was smoother, especially on 14 February (explanations for the 14 February surge will be given in the discussion section). Moreover, the daily mean light radiation curves for urban areas of several countries surrounding Ukraine were also plotted in Figure 4b.

Different from the decrease of radiation in Ukraine after the conflict, no decreasing trend of light radiation was observed in surrounding countries. Poland, Moldova, Belarus, and Romania even observed an ascent of light radiation after the outbreak of the conflict. We speculate that conflict-induced refugee migration may be responsible for the rise in radiation in these areas [46].

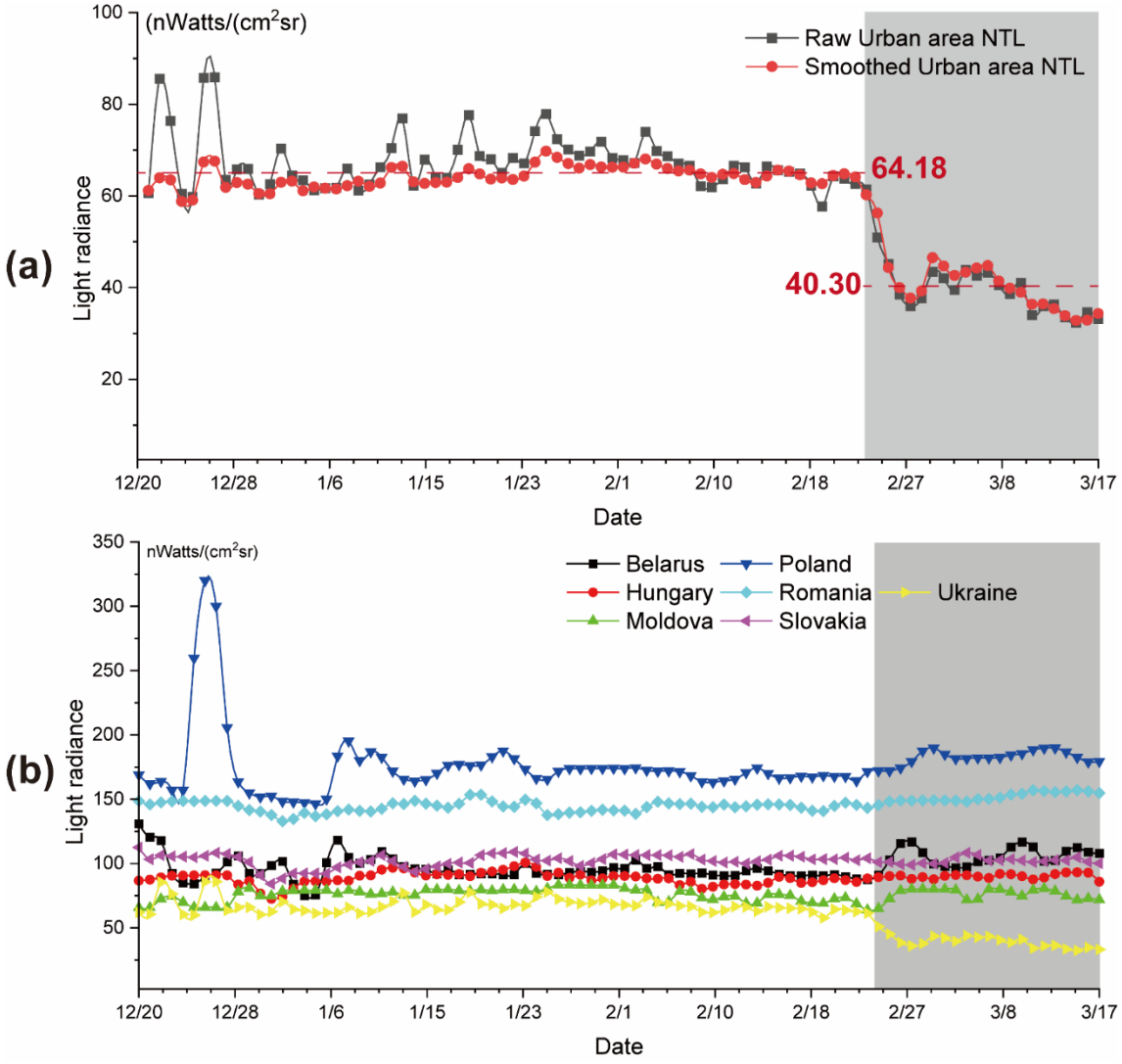

Figure 4. (**a**) Daily mean light radiation curve of the urban area of Ukraine and (**b**) Surrounding countries (gray background represents the period of conflict).

3.1.2. Identification of Power Shortage Areas

Pixel-scale Theil–Sen median trend and Mann–Kendall testing analysis of lighting dynamics can reveal a more fine-grained impact of war on the power supply. To exclude the possible increase in light emission due to the Christmas and New Year holidays, we have slightly shortened the observation period. Based on Figure 3, the observation period was defined as 15 February 2022 to 15 March 2022. Here, based on the multidimensional trend analysis tool of the ArcGIS Pro platform, the dynamic types of light radiation in Ukraine were exported, as shown in Figure 5a. It can be observed that the dramatically decreased pixels were concentrated in the urban areas of Ukraine, such as Kiev city, Kharkiv city, etc. The total area suffering from power shortages has exceeded 32,000 km^2. In addition, we still detected a few pixels with elevated light radiation in Ukraine. These strongly elevated pixels were very scattered and mainly distributed in rural and suburban areas, with a total

area of less than 1500 km^2, which was only 4% of the power shortage area. Figure 5b counts the changed pixel's area for each region. Among them, Dnipropetrovs'k possessed the most dramatically decreased pixels, covering an area of about 3100 km^2, while Kharkiv covered a similar area of about 3000 km^2, and L'viv and Kiev were closer at about 2500 km^2. Of particular interest was the capital, Kiev city, where the dramatically decreased pixels covered an area of about 1000 km^2, accounting for 60% of the total area of the region. For the dramatically increased pixels, Luhans'k reached the largest area of 402 km^2, followed by Transcarpathia and Donets'k with 190 and 110 km^2 respectively.

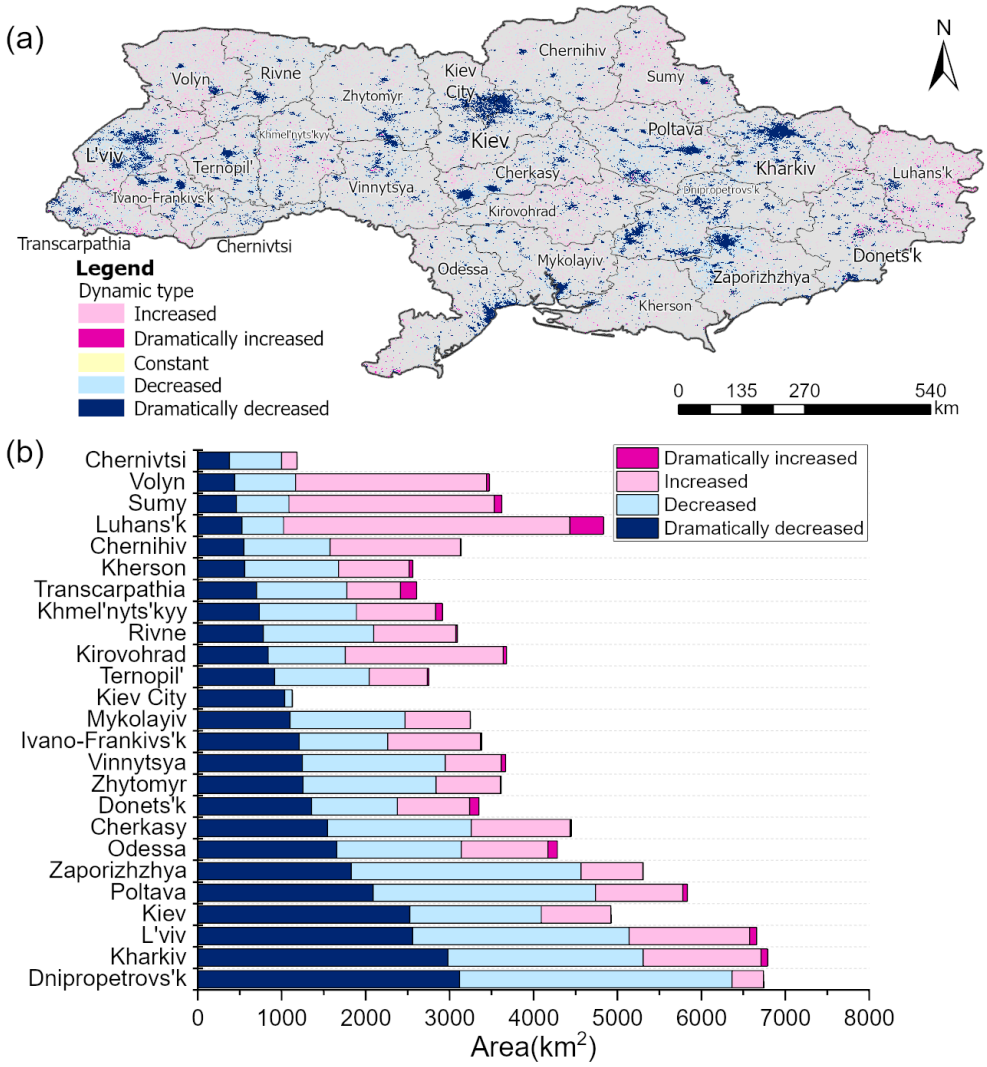

Figure 5. (**a**) Spatial distribution of the identified radiation dynamic types and (**b**) area composition for the period 15 February 2022–15 March 2022.

3.2. Estimation of the Affected Populations

3.2.1. Estimation of Total Population

The total population suffering from the power shortages was estimated based on the LandScan HD and the identified areas where the light dramatically decreased (Figure 6). Overall, the estimates show that about 17.3 million people (about 38.51% of the total population) in Ukraine live in areas that have experienced a dramatic decay in light since the outbreak of the conflict. Among them, Kharkiv and the capital Kiev city had the largest affected populations (1.69 million and 1.53 million, respectively). In addition, there were 5 oblasts with more than 1 million people affected, namely Odessa (1.34 million), L'viv (1.26 million), Kiev (1.11 million), Dnipropetrovs'k (1.11 million), and Donets'k (1.01 mil-

lion). Of the remaining eighteen oblasts, seventeen had over 0.25 million people affected. Comparatively, the Chernivtsi oblast had the lowest affected population, 0.15 million.

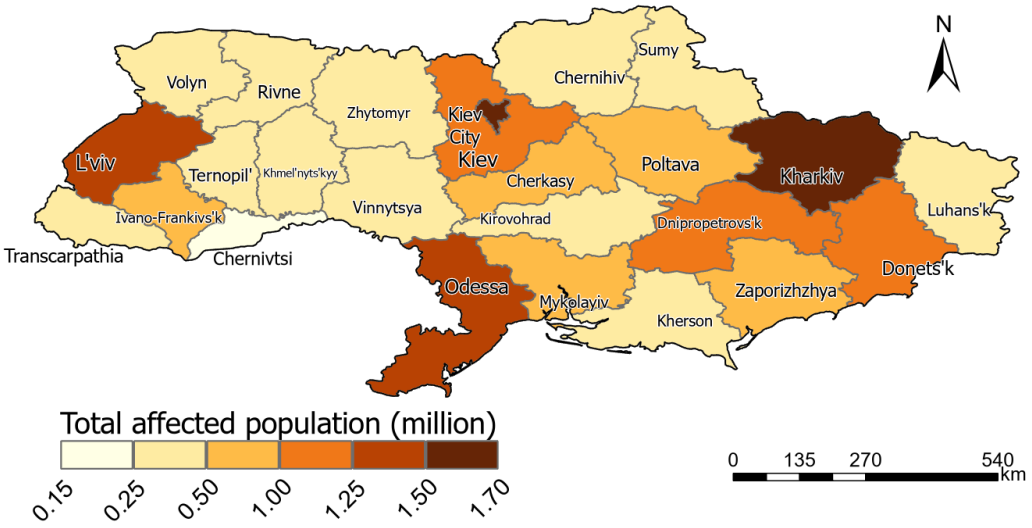

Figure 6. The estimated population within the Ukrainian oblasts affected by the power shortages triggered by the Ukrainian-Russian conflict. Specifically, the affected population for each oblast was estimated by summing up the LandScan HD layer pixel values for the deep blue (dramatically decreased) areas in Figure 5a.

3.2.2. Estimation of Vulnerable Populations

As already stated, before migrating the population profile from WorldPop GPPD to LandScan HD, the correlation between them needs to be evaluated. As shown in Figure 7a, the validation results of the two demographic products indicated their strong consistency (Pearson's r = 0.84), which ensured the migration feasibility of the population structure.

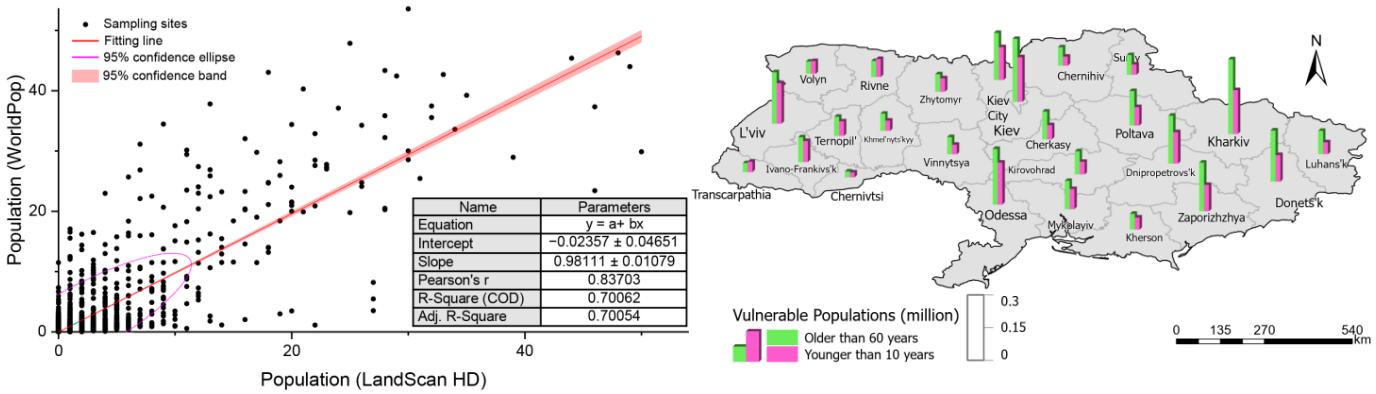

Figure 7. (**a**) Verification of population correlation from WorldPop and LandScan HD products; (**b**) The estimated affected vulnerable populations of the Ukrainian oblasts within the power shortages triggered by the Ukrainian-Russian conflict.

Based on the fused population structure data, this study estimated the vulnerable population suffering from power shortages. This information is more valuable than the total affected population, as these sensitive populations will be more likely to be adversely affected by a sharp reduction in lighting due to physical and mobility limitations and additional needs. The results suggest that the total vulnerable population suffering from power shortages in the pre-conflict period amounted to 5.88 million, accounting for 13.1% of Ukraine's total population (Figure 7b). Specifically, the population of children in Ukraine

under 10 years old who were affected was about 2.35 million (about 5.24% of the total population), while the population of elderly people over 60 years old was about 3.53 million (about 7.86% of the total population). The largest number of children affected was in Kiev city, about 205,000, while the smallest number, less than 23,000, was in Chernivtsi. In addition, Kharkiv oblast had the largest number of elderly people affected, 343,000, while Chernivtsi oblast had the smallest population, about 27,000. More-detailed statistics of the affected populations can be found in Table 1.

Table 1. Estimated population affected by power shortages (in thousands).

Name	Population	Population (Under 10)	Population (Above 60)
Kharkiv	1688	201	343
Kiev city	1530	205	289
Odessa	1336	192	255
L'viv	1261	186	236
Kiev	1107	150	215
Dnipropetrovs'k	1106	144	220
Donets'k	1011	122	234
Zaporizhzhya	964	121	223
Mykolayiv	694	93	130
Poltava	678	85	158
Ivano-Frankivs'k	629	97	114
Cherkasy	531	66	128
Luhans'k	473	55	107
Ternopil'	458	67	88
Rivne	444	82	73
Kirovohrad	441	58	106
Zhytomyr	410	62	81
Sumy	389	48	91
Kherson	381	55	72
Khmel'nyts'kyy	342	47	79
Chernihiv	335	42	85
Volyn	334	59	56
Vinnytsya	331	44	79
Transcarpathia	268	48	42
Chernivtsi	152	23	27
Total	**17,293 (38.51%)**	**2352 (5.24%)**	**3531 (7.86%)**

4. Discussion

4.1. Noise in VNP46A2 and Daily Light Radiation Tracking

Although the "Gap-Filled DNB BRDF-Corrected NTL" dataset in VNP46A2 has undergone a series of calibration processes and has been gradually used for dynamic tracking of lighting radiation for short-period events, it was still found to have some irregular background noise in its use for this paper. The increased noise tends to lead to a spike in the daily mean light radiation recorded on a large scale. For example, in Figure 3a, anomalous peaks of light radiation can be observed on 13 January, 22 January, and 13 February.

To confirm our speculation and reveal the effect of background noise on the daily mean light radiation values, a method that was previously used to remove background noise from NTL images was referenced. Specifically, based on a priori knowledge, more than 30 sample regions of theoretical "dark pixels" in the study area were selected (the extraction position of the pixels is uniform across days), which are located in mountains, forests, and large areas of water without any artificial illumination traces. Then, the mean pixel value of the "dark pixels" was calculated for each day. As shown in Figure 8, the background noise values were within 2 nWatts/cm^2/sr on most of the days across the 88-day observation period, which was consistent with the findings of previous studies [47,48]. In addition, several elevated noise incidents were observed on certain dates, such as 23 December, 12 January, 14 February, 28 February, and 16 March, with an average noise of about 4 nWatts/cm^2/sr.

Further, for the days with a surge in light radiation values (e.g., >5 nWatts/cm^2/sr) in Figure 3a, a linear correlation analysis between their light radiance and the background noise identified was performed, and the results confirmed a strong positive correlation between them with a correlation coefficient of 0.82.

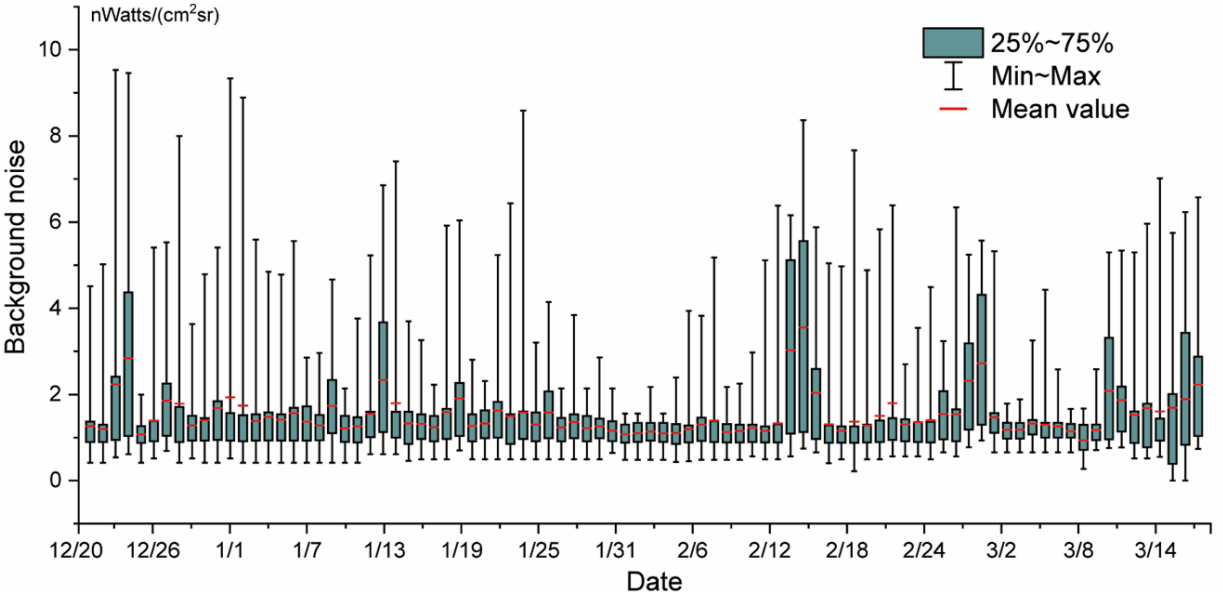

Figure 8. Daily background noise calculated based on "dark pixels" during the observation period.

In fact, a comparison of Figures 3a and 4a indicated that the background noise of VNP46A2 actually posed a more glaring risk to the monitoring of light radiation dynamics in non-urban areas, where the radiance baseline is quite low (possibly even close to the noise value), and with a wider territorial extent. Accordingly, in urban areas with limited area, due to the light radiation baseline having increased significantly, the interference of background noise on the radiation dynamics is negligible. In addition, the spatial distribution of the background noise in VNP46A2 caused by factors such as cloud cover and moonlight illumination is heterogeneous and random. Therefore, considering that conflict-induced power shortages occur mainly in urban areas, the background noise was not effectively and accurately removed in this paper.

4.2. Timely Assessment of Conflict Impacts Based on Remote Sensing Data

In this study, we used the newly developed VNP46A2 product from NASA to analyze the suppression and disturbance of human activities on the surface by war from a general perspective. During the conflict, Ukraine's major cities have experienced a significant and widespread light reduction, the reasons for which may include: (1) the destruction of electrical facilities and lighting by armed confrontation; and (2) the implementation of the nighttime curfew policy, which has been declared by the Ukrainian government several times since the outbreak of the war. In addition, we speculate that the reasons for the more considerable areas of light intensification in the Luhansk of eastern Ukraine and the Transcarpathia in the west may include: (1) for Luhansk in the east, as they were one of the first regions to be recognized as independent by Russia and being pro-Russian, additional military facilities and troop deployments probably contributed; (2) for Transcarpathia in the west, the influx of transferred refugees and the establishment of humanitarian aid centers may have led to the increased lighting emissions.

The study also introduced timely, high-precision spatial population maps to successfully estimate the population affected by power shortages. The estimated affected population is valuable to humanitarian organizations for relief and to assess the impact of the war. In fact, several previous studies have used NTL data to track war conflicts,

but our study further extends the NTL research scenario in that it can be combined with additional inputs to allow estimation of affected populations and to support humanitarian organizations in relief efforts.

4.3. Limitations

Certainly, there are still some limitations to this study. First is the background noise discussed earlier. These noise incidents may lead to an underestimation of the affected population in non-urban areas. Second, the temporal difference between LandScan HD for Ukraine and WorldPop GPPD data. Figure 7a shows that there is still some fitting difference between them, so the WorldPop GPPD-based population profile coefficients may interfere with our estimates of the vulnerable population. Third, the accuracy of the estimates of the affected population in the text has not been verified, due to the unavailability of field validation data. However, according to the latest reports by the United Nations on Ukraine, at least 7.1 million people are still displaced within the country, over 12 million people suffered from economic hardship and the decline of services, and many of them were without water and electricity [49], which is very close to the 17.3 million residents affected by the power shortages estimated in this study. Additionally, since the main purpose of this study was to explore the feasibility of rapidly assessing the induced impact of the Ukrainian-Russian conflict based on timely remote sensing data, we still believe that the timely availability and dissemination of firsthand projections of affected population from this study has a positive effect on the assessment of conflict damage and even humanitarian relief.

5. Conclusions

Since the outbreak of the Ukrainian-Russian conflict, the number of casualties continues to rise. Given that the conflict is still at a stalemate, it is very difficult to assess the impact of the conflict and the affected population based on field surveys. Therefore, based on the latest NTL products and population products, this study assesses the dynamics of lighting radiation in Ukraine and estimates the population suffering from power shortages. The results showed that (1) the average light radiation in Ukraine had decreased by about 40% since the outbreak of the war, with Kiev city recording the most dramatic decrease of about 51% after the conflict; and (2) About 17.3 million people suffered from power shortages, of which the number of children under 10 years old was about 2.35 million, while the number of elderly people aged over 60 years was about 3.53 million. The results of this study will be useful for the timely assessment of the impact of the Ukrainian-Russian conflict and for humanitarian relief.

Author Contributions: Conceptualization, Z.Z. and F.M.; methodology, Z.Z.; software, Z.Z. and C.G.; validation, Z.C., Q.Z. and Y.C.; formal analysis, G.G.; resources, Z.W.; data curation, Z.Y. and X.W.; writing—original draft preparation, Z.Z.; writing—review and editing, F.M. and Z.W.; visualization, Z.Z.; supervision, F.M., Z.C. and Z.W.; funding acquisition, Z.W. All authors have read and agreed to the published version of the manuscript.

Funding: This research was funded by the NSFC-Guangdong Joint Fund under grant U1901219; Key Special Projects for Introduced Talents Team of Southern Marine Science, Engineering Guangdong Laboratory (Guangzhou) (GML2019ZD0301); Central-Level Public Welfare Research Institutes Basic Scientific Research Special Projects (PM-zx703-202104-083); and a TESAF Research Scholarship (TESAF 2022/13).

Acknowledgments: The authors are grateful for the comments and suggestions provided by reviewers and editors.

Conflicts of Interest: The authors declare no conflict of interest.

References

1. Burki, T.K. Health of Ukranian citizens under threat from conflict and displacement. *Lancet Respir. Med.* **2022**, *10*, e49. [CrossRef]
2. Russia's war in Ukraine, Explained. Available online: https://www.vox.com/2022/2/23/22948534/russia-ukraine-war-putin-explosions-invasion-explained (accessed on 6 August 2022).
3. Haq, E.-U.; Tyson, G.; Lee, L.-H.; Braud, T.; Hui, P. Twitter dataset for 2022 russo-ukrainian crisis. *arXiv* **2022**, arXiv:2203.02955.
4. Ukraine: Civilian Casualties as of 3 July 2022. Available online: https://ukraine.un.org/en/188846-ukraine-civilian-casualties-3-july-2022 (accessed on 6 August 2022).
5. UN High Commissioner for Refugees Calls for Immediate End to Ukraine War, Which Has Uprooted Over 10 Million People. Available online: https://www.unhcr.org/news/press/2022/3/6245d8574/un-high-commissioner-refugees-calls-immediate-end-ukraine-war-uprooted.html (accessed on 6 August 2022).
6. Li, X.; Chen, F.; Chen, X. Satellite-observed nighttime light variation as evidence for global armed conflicts. *IEEE J. Sel. Top. Appl. Earth Obs. Remote Sens.* **2013**, *6*, 2302–2315. [CrossRef]
7. Li, X.; Li, D.; Xu, H.; Wu, C. Intercalibration between DMSP/OLS and VIIRS night-time light images to evaluate city light dynamics of Syria's major human settlement during Syrian Civil War. *Int. J. Remote Sens.* **2017**, *38*, 5934–5951. [CrossRef]
8. Li, X.; Liu, S.; Jendryke, M.; Li, D.; Wu, C. Night-time light dynamics during the Iraqi civil war. *Remote Sens.* **2018**, *10*, 858. [CrossRef]
9. Jiang, W.; He, G.; Long, T.; Liu, H. Ongoing conflict makes Yemen dark: From the perspective of nighttime light. *Remote Sens.* **2017**, *9*, 798. [CrossRef]
10. Zheng, Z.; Chen, Y.; Wu, Z.; Ye, X.; Guo, G.; Qian, Q. The desaturation method of DMSP/OLS nighttime light data based on vector data: Taking the rapidly urbanized China as an example. *Int. J. Geogr. Inf. Sci.* **2019**, *33*, 431–453. [CrossRef]
11. Zheng, Q.; Weng, Q.; Wang, K. Developing a new cross-sensor calibration model for DMSP-OLS and Suomi-NPP VIIRS night-light imageries. *ISPRS J. Photogramm. Remote Sens.* **2019**, *153*, 36–47. [CrossRef]
12. Xie, Z.; Ye, X.; Zheng, Z.; Li, D.; Sun, L.; Li, R.; Benya, S. Modeling polycentric urbanization using multisource big geospatial data. *Remote Sens.* **2019**, *11*, 310. [CrossRef]
13. Ma, T.; Zhou, C.; Pei, T.; Haynie, S.; Fan, J. Quantitative estimation of urbanization dynamics using time series of DMSP/OLS nighttime light data: A comparative case study from China's cities. *Remote Sens. Environ.* **2012**, *124*, 99–107. [CrossRef]
14. Wu, J.; Wang, Z.; Li, W.; Peng, J. Exploring factors affecting the relationship between light consumption and GDP based on DMSP/OLS nighttime satellite imagery. *Remote Sens. Environ.* **2013**, *134*, 111–119. [CrossRef]
15. Zhang, Q.; Seto, K.C. Mapping urbanization dynamics at regional and global scales using multi-temporal DMSP/OLS nighttime light data. *Remote Sens. Environ.* **2011**, *115*, 2320–2329. [CrossRef]
16. Zhou, Y.; Li, X.; Asrar, G.R.; Smith, S.J.; Imhoff, M. A global record of annual urban dynamics (1992–2013) from nighttime lights. *Remote Sens. Environ.* **2018**, *219*, 206–220. [CrossRef]
17. Zheng, Q.; Weng, Q.; Wang, K. Characterizing urban land changes of 30 global megacities using nighttime light time series stacks. *ISPRS J. Photogramm. Remote Sens.* **2021**, *173*, 10–23. [CrossRef]
18. Zhao, N.; Ghosh, T.; Samson, E.L. Mapping spatio-temporal changes of Chinese electric power consumption using night-time imagery. *Int. J. Remote Sens.* **2012**, *33*, 6304–6320. [CrossRef]
19. Zhao, N.; Hsu, F.-C.; Cao, G.; Samson, E.L. Improving accuracy of economic estimations with VIIRS DNB image products. *Int. J. Remote Sens.* **2017**, *38*, 5899–5918. [CrossRef]
20. Elvidge, C.D.; Baugh, K.E.; Dietz, J.B.; Bland, T.; Sutton, P.C.; Kroehl, H.W. Radiance calibration of DMSP-OLS low-light imaging data of human settlements. *Remote Sens. Environ.* **1999**, *68*, 77–88. [CrossRef]
21. Elvidge, C.D.; Baugh, K.; Zhizhin, M.; Hsu, F.C.; Ghosh, T. VIIRS night-time lights. *Int. J. Remote Sens.* **2017**, *38*, 5860–5879. [CrossRef]
22. Elvidge, C.D.; Baugh, K.E.; Kihn, E.A.; Kroehl, H.W.; Davis, E.R. Mapping city lights with nighttime data from the DMSP Operational Linescan System. *Photogramm. Eng. Remote Sens.* **1997**, *63*, 727–734.
23. Ghosh, T.; Baugh, K.E.; Elvidge, C.D.; Zhizhin, M.; Poyda, A.; Hsu, F.-C. Extending the DMSP Nighttime Lights Time Series beyond 2013. *Remote Sens.* **2021**, *13*, 5004. [CrossRef]
24. Elvidge, C.D.; Baugh, K.E.; Zhizhin, M.; Hsu, F.-C. Why VIIRS data are superior to DMSP for mapping nighttime lights. *Proc. Asia-Pac. Adv. Netw.* **2013**, *35*, 62. [CrossRef]
25. Cao, C.; Shao, X.; Uprety, S. Detecting light outages after severe storms using the S-NPP/VIIRS day/night band radiances. *IEEE Geosci. Remote Sens. Lett.* **2013**, *10*, 1582–1586. [CrossRef]
26. Zhao, X.; Yu, B.; Liu, Y.; Yao, S.; Lian, T.; Chen, L.; Yang, C.; Chen, Z.; Wu, J. NPP-VIIRS DNB daily data in natural disaster assessment: Evidence from selected case studies. *Remote Sens.* **2018**, *10*, 1526. [CrossRef]
27. Lan, T.; Shao, G.; Tang, L.; Xu, Z.; Zhu, W.; Liu, L. Quantifying spatiotemporal changes in human activities induced by COVID-19 pandemic using daily nighttime light data. *IEEE J. Sel. Top. Appl. Earth Obs. Remote Sens.* **2021**, *14*, 2740–2753. [CrossRef] [PubMed]
28. Zheng, Z.; Wu, Z.; Chen, Y.; Guo, G.; Yang, Z.; Marinello, F. A simple method for near-real-time monthly nighttime light image production. *IEEE Geosci. Remote Sens. Lett.* **2021**, *19*, 8008405. [CrossRef]
29. Xu, J.; Qiang, Y. Spatial assessment of community resilience from 2012 Hurricane Sandy using nighttime light. *Remote Sens.* **2021**, *13*, 4128. [CrossRef]

30. Wang, Z.; Román, M.; Sun, Q.; Molthan, A.; Schultz, L.; Kalb, V. Monitoring disaster-related power outages using NASA black marble nighttime light product. In Proceedings of the The International Archives of the Photogrammetry, Remote Sensing and Spatial Information Sciences, Beijing, China, 7–10 May 2018; pp. 1853–1856.
31. Xu, G.; Xiu, T.; Li, X.; Liang, X.; Jiao, L. Lockdown induced night-time light dynamics during the COVID-19 epidemic in global megacities. *Int. J. Appl. Earth Obs. Geoinf.* **2021**, *102*, 102421. [CrossRef]
32. Wang, Z.; Shrestha, R.M.; Román, M.O.; Kalb, V.L. NASA's Black Marble multi-angle nighttime lights temporal composites. *IEEE Geosci. Remote Sens. Lett.* **2022**, *19*, 2505105. [CrossRef]
33. Ukraine Country Profile. Available online: https://www.bbc.com/news/world-europe-18018002 (accessed on 26 July 2022).
34. Zheng, Q.; Weng, Q.; Zhou, Y.; Dong, B. Impact of temporal compositing on nighttime light data and its applications. *Remote Sens. Environ.* **2022**, *274*, 113016. [CrossRef]
35. LandScan High Definition Data for Ukraine, January 2022. Available online: https://developers.google.com/earth-engine/datasets/catalog/DOE_ORNL_LandScan_HD_Ukraine_202201 (accessed on 6 August 2022).
36. WorldPop Global Project Population Data: Estimated Age and Sex Structures of Residential Population per 100 × 100 m Grid Square. Available online: https://developers.google.com/earth-engine/datasets/catalog/WorldPop_GP_100m_pop_age_sex#description (accessed on 6 August 2022).
37. Reid, S.; Weber, E.; Moehl, J.; Cooper, J.A.; Levy, C. Fusing Land Use Data and Population Density Estimates for High Resolution Population Modeling: LandScan HD. In Proceedings of the AGU Fall Meeting Abstracts, Washington, DC, USA, 10–14 December 2018; p. IN33B-0846.
38. Rose, A.; McKee, J.; Weber, E.; Bhaduri, B.L. Geoscience meets social science: A flexible data driven approach for developing high resolution population datasets at global scale. In Proceedings of the AGU Fall Meeting Abstracts, New Orleans, LO, USA, 11–15 December 2017; p. IN51H-04.
39. WorldPop Methods. Available online: https://www.worldpop.org/methods/ (accessed on 26 July 2022).
40. Xu, P.; Wang, Q.; Jin, J.; Jin, P. An increase in nighttime light detected for protected areas in mainland China based on VIIRS DNB data. *Ecol. Indic.* **2019**, *107*, 105615. [CrossRef]
41. Zheng, Z.; Wu, Z.; Chen, Y.; Guo, G.; Cao, Z.; Yang, Z.; Marinello, F. Africa's protected areas are brightening at night: A long-term light pollution monitor based on nighttime light imagery. *Glob. Environ. Chang.* **2021**, *69*, 102318. [CrossRef]
42. Tucker, C.; Newcomb, W.; Los, S.; Prince, S. Mean and inter-year variation of growing-season normalized difference vegetation index for the Sahel 1981–1989. *Int. J. Remote Sens.* **1991**, *12*, 1133–1135. [CrossRef]
43. Liu, Z.; Wang, Y.; Yao, Z.; Kang, H. Trend and periodicity of precipitation, air temperature and runoff in the Taihu Lake Basin. *J. Nat. Resour.* **2011**, *26*, 1575–1584. [CrossRef]
44. The Impact of War on Older People (In Ukraine and Everywhere Else). Available online: https://www.helpage.org/newsroom/latest-news/the-impact-of-war-on-older-people-in-ukraine-and-everywhere-else/ (accessed on 6 August 2022).
45. De Alencar Rodrigues, J.A.R.; Lima, N.N.R.; Neto, M.L.R.; Uchida, R.R. Ukraine: War, bullets, and bombs-millions of children *Pl*and adolescents are in danger. *Child. Abus. Neglect.* **2022**, *128*, 105622. [CrossRef] [PubMed]
46. Ukraine Refugee Situation. Available online: https://data.unhcr.org/en/situations/ukraine (accessed on 6 August 2022).
47. Li, X.; Zhou, Y.; Zhao, M.; Zhao, X. A harmonized global nighttime light dataset 1992–2018. *Sci. Data* **2020**, *7*, 1–9. [CrossRef]
48. Wu, K.; Wang, X. Aligning pixel values of DMSP and VIIRS nighttime light images to evaluate urban dynamics. *Remote Sens.* **2019**, *11*, 1463. [CrossRef]
49. The UN Reiterates the Call for an Easter Truce in Ukraine Amid a Growing Humanitarian Crisis and Mounting Displacement. Available online: https://ukraine.un.org/en/178431-un-reiterates-call-easter-truce-ukraine-amid-growing-humanitarian-crisis-and-mounting (accessed on 6 August 2022).